Bending of Fibre Reinforced Thermoplastic Sheets

T A Martin, D Bhattacharyya and I F Collins
School of Engineering, University of Auckland, New Zealand

ABSTRACT

When forming continuous fibre reinforced thermoplastic (CFRT) sheets into 3-D components, interply shearing may be necessary in order to accommodate the out-of plane bending because the fibres severely constrain the deformation along the fibre directions within their planes. Furthermore, thermoforming takes place at elevated temperatures so that the molten matrix polymer becomes fluid. These two factors are of prime importance in analysing any forming process with thermoplastic composite materials. This paper examines the process of forming unidirectional PLYTRON® (a glass-fibre reinforced polypropylene composite, originally developed by ICI, UK) sheets into V-bends at a constant elevated temperature, and compares the experimental results with those predicted by an analytical model for plane strain bending of an incompressible Newtonian fluid reinforced with a single family of inextensible fibres. The shape of a strip as it is formed, the effects of temperature and forming speed on the forming loads are also investigated. A major conclusion from this study is that PLYTRON sheets demonstrate a visco-elastic response when formed within their melting range and the degree of elasticity is increased by reducing the temperature, which, in turn, can reduce the fibre instability. The theoretical model provides useful results for evaluating the effects of forming speed and punch geometry on the bending stresses in such sheets and also highlights the limitations of a Newtonian fluid model in comparison with the actual material response.

Keywords: *vee bending, continuous fibre reinforced thermoplastic sheets, visco-elastic, kinematic model, admissible stress field*

1 Introduction

In any forming operation, where a flat sheet is to be transformed into a 3-D component, out-of-plane bending is inevitable. However, in many cases the principal surface curvatures are small except in some localised regions. Consequently, most sheet metal forming operations are often treated as in-plane stretching processes, while out-of-plane shear deformations are largely ignored for simplicity of analysis. In regions of severe bending, the circumferential strain is assumed to vary linearly through the thickness of the sheet and the surface normal is taken as the third principal direction of strain. In the case of reinforced thermoplastics, with high loadings of continuous or long fibres, these assumptions are not valid. In fact, even a single-bend operation necessitates interply shear, unless the fibres are aligned with the bend axis, since the layers of fibres resist in-plane deformations along their lengths [1].

This paper examines the subject of forming CFRT composites into V-bends at elevated temperatures in order to observe the deformation mechanisms in a relatively simple single-axis bend. The three main objectives are: (a) to observe the shapes of some unidirectional PLYTRON strips as they are free formed under isothermal conditions in a three point bending device, (b) to measure the experimental loads required to form the strips, and (c) to compare these results with an idealised beam bending model for an incompressible viscous fluid reinforced with a single family of inextensible fibres. Several researchers have manufactured V bends using both cold and hot matched face dies in order to understand the practical problems with forming such sections [2-4]. In Soll's paper [2], a model for bending a laminate of elastic layers separated by thin viscous fluid layers is developed; however, no attempt is made to establish an analytical load/displacement relationship based on a theoretically derived strip deflection curve. One way to simplify the analysis of CFRT materials is to assume an idealised behaviour by imposing suitable kinematic constraints on a continuum model. A few authors have recently published theoretical solutions for bending fibre reinforced elastic, plastic and linearly viscoelastic cantilever beams subjected to two kinematic constraints; fibre inextensibilty and incompressibility [5-7]. An earlier paper by Rogers and O'Neill [8] deals specifically with a viscous fluid model using these constraints. In this paper, an idealised material model for an incompressible viscous fluid reinforced with inextensible fibres is also utilised. In addition, a plane strain constraint allows a purely kinematic approach to be taken for generating solutions to forming problems. In simple cases kinematically admissible shapes may be readily established and, provided the boundary conditions are satisfied, the solution is also statically admissible. When dealing with a viscous material the solution is time dependent and, for three point bending, the boundary conditions change with time as the strip is drawn into the

deformation zone. In spite of these difficulties, a theory for plane strain bending of a unidirectional laminate has been developed which yields an analytical solution for small deflections. A numerical solution for the complete forming of such a material could be developed, but that approach has been left for a later date. The analytical model yields a straightforward interpretation of the effects of forming speed and die geometry on the bending stresses in a real sheet during forming, and provides an excellent basis for further work with a non-linear viscoelastic material model.

2 Development of a Viscous Fluid Beam Bending Model

Thermoplastic polymers are known to exhibit viscous behaviour when formed at temperatures within or above their melting ranges. The matrix material in a CFRT composite sheet may therefore be idealised as an incompressible Newtonian fluid in its molten state. In addition, the fibres severely limit deformations along their lengths and these can be treated as thin homogeneously distributed inextensible cords. In the current section we consider plane strain bending of an initially flat plate with uniaxial fibre reinforcement in its plane. The fibres lie perpendicular to the bend axis when the sheet is subjected to three point loading, as shown in Figure 1. Many of the mathematical derivations presented in the following theoretical model can be found in Spencer's text [9].

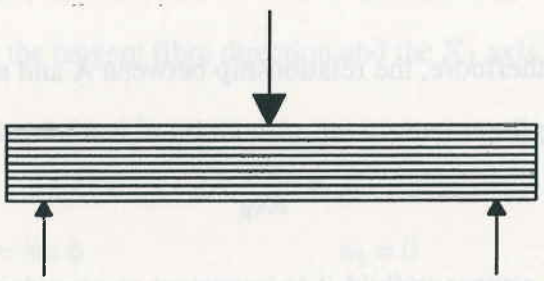

Figure 1: Three point bending of an incompressible inextensible beam.

2.1 Constraint Conditions and Kinematics

The first two considerations regarding this idealised material concern the kinematic constrains imposed on any deformation by the assumptions of incompressibility and fibre inextensibility. In the following analysis capital letters indicate vector quantities referred to the undeformed configuration, whereas small letters indicate vector quantities referenced to the deformed state. In a Cartesian reference frame the incompressibility constraint may be expressed mathematically as

$$\frac{\partial v_i}{\partial x_i} = d_{ii} = 0, \qquad \text{or} \qquad \det\left|\frac{\partial x_i}{\partial X_i}\right| = 1 \qquad (1)$$

where **x** and **X** refer to the deformed and undeformed coordinate vectors of a material particl respectively, **v** is the velocity vector, and d_{ij} is the rate of deformation tensor defined by

$$d_{ij} = \frac{1}{2}\left(\frac{\partial v_i}{\partial x_j} + \frac{\partial v_j}{\partial x_i}\right) \qquad (2)$$

In a continuum, a family of fibres may be characterised by a field of unit tangent vectors. In th reference configuration these may be represented by a unit vector field $A(X_R)$. The fibr direction at any particle is then the direction of **A**. Therefore, the trajectories of **A** represent th fibres themselves and the components of **A** are denoted by A_R. During a deformation the fibre will be convected with the continuum and the same particles will lie on a given fibre at an time, t. The new fibre paths may then be represented by the trajectories of a new unit vecto field $\mathbf{a}(X_R,t)$. Using these definitions the fibre inextensibility condition may be written as

$$a_i a_j \frac{\partial v_i}{\partial x_j} = a_i a_j d_{ij} = 0, \qquad \text{or} \qquad \frac{\partial x_i}{\partial X_R}\frac{\partial x_i}{\partial X_S} A_R A_S = 1 \qquad (3)$$

Furthermore, the relationship between **A** and **a** on an inextensible fibre is expressed by

$$a_i = \frac{\partial x_i}{\partial X_R} A_R \qquad (4)$$

For a viscous fluid it is important to consider the time rate of change of **a.** By differentiating the equation (4) with respect to time and keeping X_R constant, the material derivative, $\dot{a}_i$, is also readily obtained.

$$\dot{a}_i = a_k \frac{\partial v_i}{\partial x_k} \qquad (5)$$

The only other constraint imposed on the deformation is that of plane strain. At this point it is necessary to consider a series of **n**-lines, which represent orthogonal trajectories to the **a**-lines. These lines are not material curves in general, because particles lying on a normal line before deformation will not necessarily lie on the same normal line after deformation. Pipkin and Rogers [10] have derived the theory for plane strain deformations of incompressible, inextensible materials. In the present analysis a plate of uniform thickness is considered, in which the fibres all lie in parallel surfaces in the plane of deformation. Two significant kinematic results which follow from Pipkin and Rogers' analysis are summarised as follows.

(a) If the **a**-lines are initially parallel, the **n**-lines must be initially straight and must remain straight throughout any plane strain deformation. Thus, the fibres remain in parallel surfaces.

(b) The normal distance between any two adjacent fibres must be constant at all points along that pair. Therefore, the thickness of the sheet cannot change during plane strain deformation.

These two requirements permit only simple shear deformations along the fibres and the amount of shear is conveniently expressed by the change in angle between two adjacent fibres Consider Figure 2(a, b), in which an initially flat plate is deformed by shear. Rigid body rotations and translations are ignored. In the (x_1,x_2) plane, the **A** vector represents the undeformed fibres as a family of **A**-curves and the **N** vector represents a family of curves normal to the A-curves. These two families have the vector components

$$\begin{aligned} A_1 &= \cos\Phi & A_2 &= \sin\Phi & A_3 &= 0 \\ N_1 &= -\sin\Phi & N_2 &= \cos\Phi & N_3 &= 0 \end{aligned} \qquad (6)$$

where Φ represents the initial angle between the tangent fibre direction and the X_1 axis.

Analogous **a**-curves and **n**-curves may also be defined in relation to the current configuration. Their components are given by

$$\begin{aligned} a_1 &= \cos\phi & a_2 &= \sin\phi & a_3 &= 0 \\ n_1 &= -\sin\phi & n_2 &= \cos\phi & n_3 &= 0 \end{aligned} \qquad (7)$$

where ϕ represents the current angle between the tangent fibre direction and the x_1 axis.

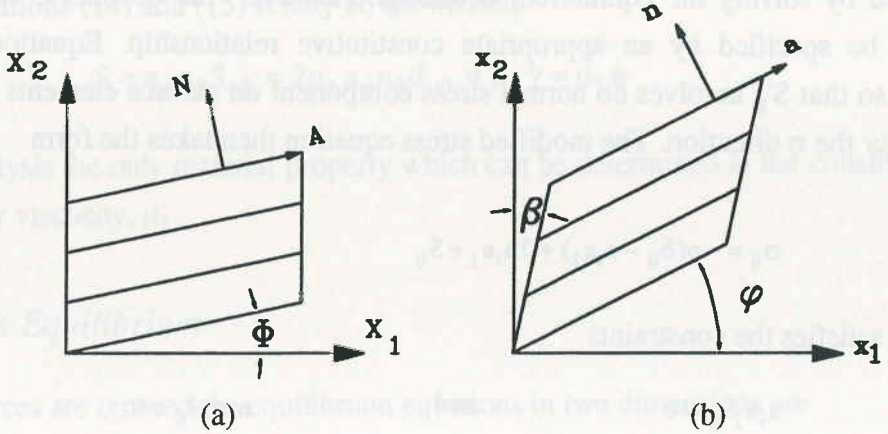

(a) (b)

Figure 2: (a) Undeformed element, (b) Element after deformation.

The shear angle, γ, may be expressed simply as

$$\gamma = \phi - \Phi + \beta \tag{8}$$

where β is a constant along each **a**-line. See Spencer [9] for full details.

If the fibres are embedded at one end, or a line of symmetry exists along which there is no shear deformation, β=0 for each fibre throughout the entire deformation. Since Φ is a constant the shear rate, $\dot{\gamma}$, may be expressed in terms of ϕ as,

$$\dot{\gamma} = \dot{\phi} \tag{9}$$

This result is useful when establishing a constitutive relationship for a viscous material.

2.2 Stress in a constrained material

The next important step in this analysis involves the introduction of a stress tensor which divides the stress into two distinct parts. The total stress in a constrained material can be thought of as the sum of a reaction stress, r'_{ij}, and an extra stress, S'_{ij}.

$$\sigma_{ij} = -p'\delta_{ij} + T'a_i a_j + S'_{ij} \tag{10}$$

The reaction stress does no work in a deformation and the reactions p' and T', in (10), arise as a result of the incompressibility and fibre inextensibility constraints. These scalar terms must be determined by solving the equilibrium equations. However, the deviatoric stress tensor, S'_{ij} needs to be specified by an appropriate constitutive relationship. Equation (10) may be rewritten so that S'_{ij} involves no normal stress component on surface elements normal to the **a** direction or the **n** direction. The modified stress equation then takes the form

$$\sigma_{ij} = -p(\delta_{ij} - a_i a_j) + Ta_i a_j + S_{ij} \tag{11}$$

where S_{ij} satisfies the constraints

$$a_i a_j S_{ij} = 0 \qquad \text{and} \qquad n_i n_j S_{ij} = 0 \tag{12}$$

Now, p represents the total pressure on elements normal to the **n** direction and T is the total tension on elements normal to the fibre direction. If the material has reflectional symmetry in the x_3 plane and the deformation is homogeneous, under plane strain conditions the only non-zero components of σ_{ij} are

$$\sigma_{\alpha\beta} = -p(\delta_{\alpha\beta} - a_\alpha a_\beta) + Ta_\alpha a_\beta + S_{\alpha\beta} \qquad (\alpha,\beta = 1,2)$$

and $$\sigma_{33} = -p + S_{33} \qquad (13)$$

A constitutive relationship is required to define S_{33} and $S_{\alpha\beta}$. If $S_{\alpha\beta}$ is now resolved into components referred to rectangular cartesian coordinates in the **a** and **n** directions, the only non-zero term arising in the stress tensor is a shear stress, S, along the fibre direction. Therefore

$$S_{\alpha\beta} = S(a_\alpha n_\beta + n_\alpha a_\beta) \qquad (14)$$

2.3 Constitutive Equation

In the present analysis, the deformation of an incompressible Newtonian fluid reinforced with a single family of inextensible fibres in the (x_1,x_2) plane is considered. According to Rogers [11], the constitutive relationship for a linear viscous fluid subjected to these two constraints is given by

$$S_{\alpha\beta} = 2\mu_T d_{\alpha\beta} + 2(\mu_L - \mu_T)(a_\alpha a_\kappa d_{\kappa\beta} + a_\beta a_\kappa d_{\kappa\alpha})$$

and $$S_{33} = 2\mu_T d_{33} \qquad (15)$$

where μ_L and μ_T are the respective viscosities of the continuum along and transverse to the fibres. In a plane strain deformation, $v_3=d_{33}=0$. Therefore, from (13), $\sigma_{33}=-p$. Hence, a stress must be applied normal to the plane of deformation to maintain the plane strain condition.

Using equations (14) and (15) it may be shown that

$$S = a_\alpha n_\beta S_{\alpha\beta} = 2\mu_L a_\alpha n_\beta d_{\alpha\beta} = \mu_L \dot{\gamma} = \mu_L \dot{\phi} \qquad (16)$$

In this analysis the only material property which can be determined in the constitutive equation is the shear viscosity, μ_L.

2.4 Stress Equilibrium

If body forces are ignored the equilibrium equations in two dimensions are

$$\frac{\partial \sigma_{\alpha\beta}}{\partial x_\beta} = 0 \qquad (17)$$

After substituting $\sigma_{\alpha\beta}$ from (13) into (17) and resolving the two equations along the **a** and **n** directions, remembering that k_a is the curvature along the **a** direction and $k_n=0$, we obtain

$$\frac{\partial T}{\partial \xi}+\frac{\partial S}{\partial \eta}-2k_aS=0$$

and

$$\frac{-\partial p}{\partial \eta}+(T+p)k_a+\frac{\partial S}{\partial \xi}=0 \qquad (18)$$

where $\partial/\partial\xi$ represents partial differentiation along a fibre line and $\partial/\partial\eta$ represents partial differentiation along a normal line. Using equation (18), T and p may be determined after S is calculated from the deformation gradients. In a straight section $k_a=0$.

In curved sections it is sometimes convenient to introduce a quasi-polar coordinate system as shown in Figure 3, where η is the normal distance between a given **a**-line and a reference **a**-line ($\eta=0$) and ϕ is the angle that the **n**-line makes with a fixed direction $\phi=0$. The governing differential equations then become.

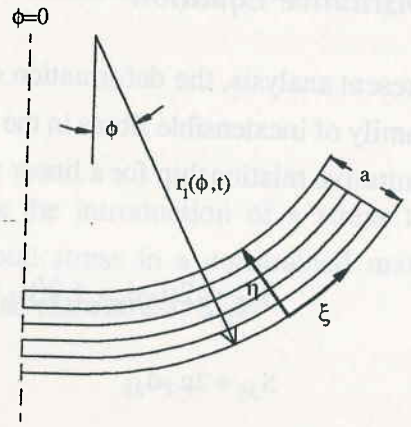

Figure 3: Quasi-polar coordinate system

$$\frac{\partial T}{\partial \phi}=-r\frac{\partial S}{\partial \eta}+2S$$

and

$$-r\frac{\partial p}{\partial \eta}+T+p=-\frac{\partial S}{\partial \phi} \qquad (19)$$

where $r(\phi,t)=r_1(\phi,t)-\eta$

We may also introduce some force resultants, S* and T*, which are defined as the resultant shear and tensile forces per unit length in the **k** direction, acting across a normal line ϕ=constant:

$$S^*=\int_0^a S\,d\eta \qquad \text{and} \qquad T^*=\int_0^a T\,d\eta \qquad (20)$$

Equations (19) can then be integrated to give

$$\frac{\partial T^*}{\partial \phi} - S^* = r_1 S_1 - r_0 S_2$$

and

$$T^* + \frac{\partial S^*}{\partial \phi} = -r_1 p_1 + r_0 p_0 \qquad (21)$$

where the boundary shear traction and pressure are $S_0(\phi)$, $p_0(\phi)$ on $r = r_0(\phi,t) = r_1(\phi,t)$-a and $S_1(\phi)$, $p_1(\phi)$ on $r = r_1(\phi,t)$. In this analysis there are no shear tractions on the surface of the sheet, so $S_0 = S_1 = 0$ always, and all surface loads are applied on the surface r_0, so $p_1 = 0$.

2.5 Plane Strain Velocity Field

In plane strain we have $v_1 = v_1(x_1,x_2)$, $v_2 = v_2(x_1,x_2)$, $v_3 = 0$

The constraint conditions (1) and (3) then become

$$\frac{\partial v_1}{\partial x_1} + \frac{\partial v_2}{\partial x_2} = 0 \qquad (22)$$

and

$$\cos^2\phi \frac{\partial v_1}{\partial x_1} + \sin\phi\cos\phi\left(\frac{\partial v_1}{\partial x_2} + \frac{\partial v_2}{\partial x_1}\right) + \sin^2\phi \frac{\partial v_2}{\partial x_2} = 0 \qquad (23)$$

These two equations are similar to those used for plane strain slip line theory in plasticity, and lead to Geiringer's equations [12].

$$\frac{\partial v_a}{\partial \xi} - v_n \frac{\partial \phi}{\partial \xi} = 0, \qquad \frac{\partial v_n}{\partial \eta} + v_a \frac{\partial \phi}{\partial \eta} = 0 \qquad (24)$$

where v_a, v_n denote the velocity components along the **a**-curves and **n**-curves respectively, and $\partial/\partial\xi$, $\partial/\partial\eta$ represent differentiation with respect to the arc lengths along these curves. In this theory, ϕ represents the angle between the fibre tangent direction and the x_1 axis.

Also, using equation (5), it may be shown that

$$\dot{\phi} = \frac{\partial v_n}{\partial \xi} + v_a \frac{\partial \phi}{\partial \xi} = \frac{1}{r}\left(\frac{\partial v_n}{\partial \phi} + v_a\right) \qquad (25)$$

2.6 Deformation of a flat plate

Consider a flat section, as shown in Figure 4, which carries no loads on its boundary surfaces. The shear force is constant between the load supports; therefore, S* = P/2.

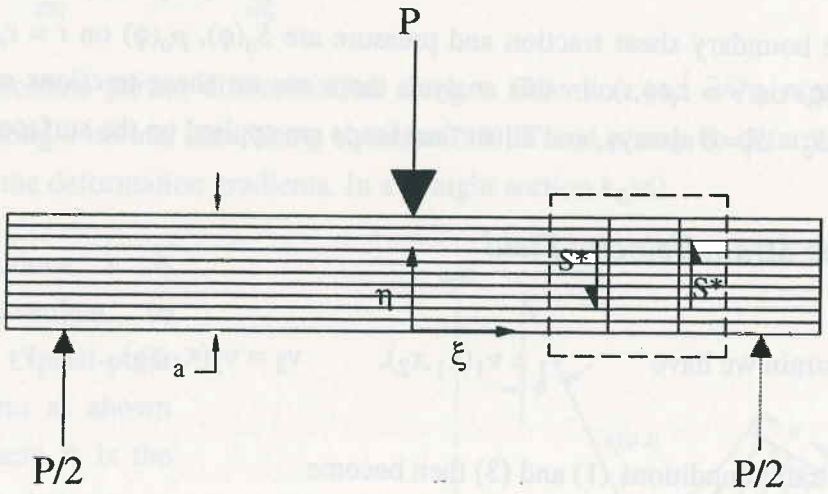

Figure 4: Three point bending of a flat plate.

Because ϕ is constant along any normal line, $\partial\phi/\partial\eta = 0$. Therefore, from the second equation of (24), $v_n = f(\xi)$. In a straight section, $\partial\phi/\partial\xi = 0$ and, using (25),

$$\dot{\phi} = \frac{\partial v_n}{\partial \xi} = f'(\xi) \tag{26}$$

So $\dot{\phi}$ is constant through the thickness of the sheet and, from (20),

$$S^* = \int_0^a S\, d\eta = \int_0^a \mu_L \phi\, d\eta = a\mu_L \phi = \frac{P}{2} \tag{27}$$

Therefore, $$\phi = \frac{P}{2a\mu_L} \tag{28}$$

Thus, $\dot{\phi}$ is constant along the length of the straight section between the boundary loads. In this region the fibres all rotate at the same rate and straight fibres remain straight.

2.7 Kinematic Model for a V-bend

The following kinematic solution is proposed for the shape of the deformed region in a flat strip subjected to three point bending. Because the bending is symmetrical about the punch, a geometric construction for only one half of the deformed strip is shown in Figure 5. With progressive deformation, fan regions grow beneath the nose of the punch and at the end supports. The region between the punch and the support remains straight, and there is no shear deformation outside of the load supports.

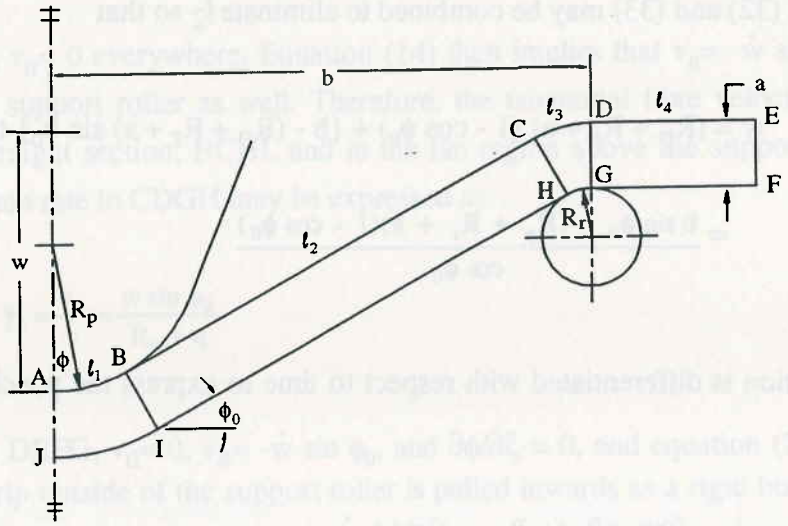

Figure 5: V-bend deformation model.

The half-strip of length L/2, shown in Figure 5, has been divided into four main sections: ℓ_1 represents the fibre length in the fan region at the inside radius of the punch, ℓ_3 represents the fibre length in the fan region at the outside radius of the support roller, ℓ_2 represents the fibre length in the straight section between these two fan regions and ℓ_4 represents the fibre length outside the support roller. From these definitions the following simple geometric expressions may be written.

$$\frac{L}{2} = \ell_1 + \ell_2 + \ell_3 + \ell_4 \tag{29}$$

$$\ell_1 = \phi_0 R_p \tag{30}$$

$$\ell_3 = \phi_0 (R_r + a) \tag{31}$$

The distance between the support roller and the punch, b, may be expressed as

$$b = (R_p + R_r + a)\sin\phi_0 + \ell_2\cos\phi_0 \qquad (32)$$

and the punch displacement, w, is given by

$$w = (R_p + R_r + a)(1 - \cos\phi_0) + \ell_2\sin\phi_0 \qquad (33)$$

Equations (32) and (33) may be combined to eliminate ℓ_2 so that

$$w = (R_p + R_r + a)\,(1 - \cos\phi_0) + \{b - (R_p + R_r + a)\sin\phi_0\}\tan\phi_0$$

$$= \frac{b\sin\phi_0 - (R_p + R_r + a)(1 - \cos\phi_0)}{\cos\phi_0} \qquad (34)$$

This equation is differentiated with respect to time to express the punch velocity, $\dot{w}$, in terms of $\dot{\phi}_o$ as

$$\dot{w} = \dot{\phi}_0\left(\frac{b - (R_p + R_r + a)\sin\phi_0}{\cos^2\phi_0}\right) \qquad (35)$$

Now consider section ABIJ in Figure 5. The normal and tangential velocities, v_a and v_n, are

$$v_a = -\dot{w}\sin\phi \qquad \text{and} \qquad v_n = -\dot{w}\cos\phi$$

and, from (25),

$$\dot{\gamma}_1 = \frac{1}{r}\left(\frac{\partial v_n}{\partial\phi} + v_a\right) = 0 \qquad (36)$$

Hence, the rate of shear deformation beneath the punch nose is zero. This fan region simply moves downwards like a rigid body.

In region BCHI the strip remains straight and the shear strain rate, $\dot{\gamma}$, is equal to the rate of rotation of the strip, $\dot{\phi}_0$. Using equations (35) and (25),

$$\dot{\gamma}_2 = \dot{w}\left(\frac{\cos^2\phi_0}{b - (R_p + R_r + a)\sin\phi_0}\right) = \frac{\partial v_n}{\partial \xi} \qquad (37)$$

This shows that the shear rate changes as the punch depth increases, but does not vary along the straight section. Consequently, v_n varies linearly along length ℓ_2 and is zero at point H. In this straight region $\partial\phi/\partial\xi = 0$ and, using equation (24),

$$\frac{\partial v_a}{\partial \xi} = 0 \qquad \text{which integrates to give} \qquad v_a = -\dot{w}\sin\phi_0 \qquad (38)$$

In region CDGH, $v_n = 0$ everywhere. Equation (14) then implies that $v_a = -\dot{w}\sin\phi_0$ in the fan region above the support roller as well. Therefore, the tangential fibre velocity, v_a, remains constant in the straight section, BCHI, and in the fan region above the support roller. Using (17), the shear strain rate in CDGH may be expressed as

$$\dot{\gamma}_3 = \frac{v_a}{r} = \frac{\dot{w}\sin\phi_0}{R_r + \eta} \qquad (39)$$

Finally, in section DEFG, $v_n = 0$, $v_a = -\dot{w}\sin\phi_0$, and $\partial\phi/\partial\xi = 0$, and equation (25) implies that $\dot{\gamma}_4 = 0$ too. The strip outside of the support roller is pulled inwards as a rigid body. There is no work done in this section. Consequently, length ℓ_4 may extend to infinity, since it has no effect on the theoretical load required to form the V-bend.

2.8 Admissible Stress Fields

The previously kinematically admissible results automatically lead to an admissible stress field solution, which admits stress discontinuities across **a**-lines and **n**-lines in order to satisfy the boundary conditions.

In sections DEFG and ABIJ, $\dot{\gamma}=0$, which means that $S_1=S_4=0$. In section BCHI, from equations (20) and (37),

$$S_2^* = \int_0^a \mu_L \dot{\gamma}_2 d\eta = \mu_L a\dot{w}\left(\frac{\cos^2\phi_0}{b - (R_p + R_r + a)\sin\phi_0}\right) \qquad (40)$$

and in section CDGH, from equations (20) and (39),

$$S_3^* = \int_0^a \mu_L \dot{\gamma}_3 d\eta = \int_0^a \frac{\mu_L \dot{w} \sin\phi_0}{R_r + a - \eta} d\eta = \ln\left(1 + \frac{a}{R_r}\right) \mu_L \dot{w} \sin\phi_0 \qquad (41)$$

Figure 6 shows the variation in the resultant shear force as a function of the arc length along an **a**-line. Clearly, the resultant shear force is discontinuous across **n**-lines; BI, CH and DG. This is possible, provided point loads are applied on the surface at points B, C, D, I, H, or G, with force magnitudes equal to the jump in shear stress across each line of discontinuity.

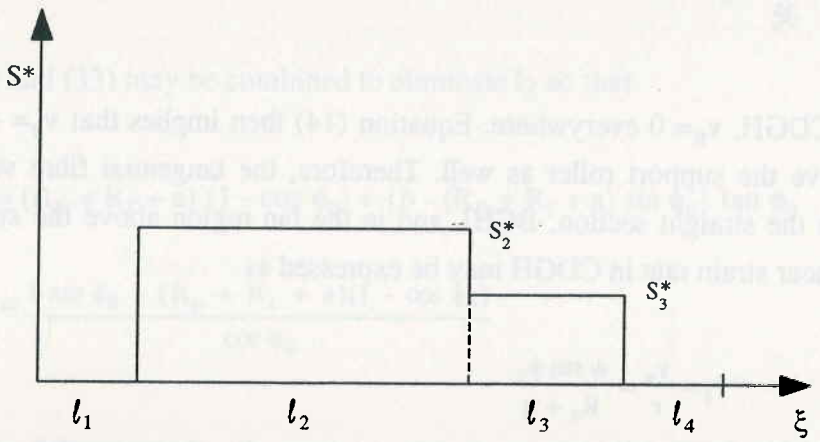

Figure 6: Resultant shear force along the length of the beam.

If we consider the equilibrium of element CDGH the total force acting on the support roller and the resultant normal force in the sheet can be calculated. Along the line EF there is no applied traction, so T=0 there. As there is no deformation in the section outside of the supports, the normal force resultant remains zero up to line DG. Upon crossing line DG there is jump in shear stress equal to S^*_3. This jump in shear stress is always positive and the roller applies a reaction load at point G of magnitude S^*_3. If the roller is frictionless, using the first equation of (21) and equation (41),

$$\frac{\partial T^*}{\partial \phi} = S^* = \ln\left(1 + \frac{a}{R_r}\right) \mu_L \dot{w} \sin\phi_0 \quad \Rightarrow \quad T^* = \phi \ln\left(1 + \frac{a}{R_r}\right) \mu_L \dot{w} \sin\phi_0 \qquad (42)$$

Thus, the resultant force increases from zero at the free edge, DG, up to a maximum tensile value, T^*_0, at $\phi=\phi_0$. The resultant shear and normal forces also give rise to a distributed load on the surface of the roller, p_0, which may be calculated from the second equation of (21).

$$p_0 = \frac{T^*}{r_0} = \phi \ln\left(1 + \frac{a}{R_r}\right) \frac{\mu_L \dot{w} \sin\phi_0}{R_r} \qquad (43)$$

This distributed load is also always positive and increases from zero at point G to a maximum at H. Upon crossing line CH there is a jump in shear stress equal to S^*_3-S^*_2. As long as $S^*_3 > S^*_2$, the roller provides a positive reaction force at point H equal to the jump in shear stress there. In the straight section, BCHI, the shear force, S^*_2, and the normal force, T^*_0, remain constant along length ℓ_2. Beneath the punch nose, in section ABIJ, $\dot{\gamma} = 0$ and $S^*_1 = 0$; so, there is a negative jump in shear stress across line BI. A reaction force of magnitude S^*_2 must therefore be applied by the punch at point B. If the punch is assumed to be frictionless, there is no shear traction on the inside bend radius so that equations (21) and (36) lead to the following result:.

$$\frac{\partial T^*}{\partial \phi} = 0 \qquad \text{and hence} \qquad T^* = T^*_0 \tag{44}$$

This normal force gives rise to a uniformly distributed load on the surface of the punch, p_0. From equation (21),

$$p_0 = \frac{T^*}{r_0} = \frac{T^*_0}{R_p} = \frac{\mu_L \dot{w} \phi_0 \sin\phi_0}{R_p} \ln\left(1 + \frac{a}{R_r}\right) \tag{45}$$

The net downward load on the punch can now be determined from the resultant shear force, S^*_2, and the resultant normal force, T^*_0, in the straight section of the beam,

$$\frac{P}{2} = S^*_2 \cos\phi_0 + T^*_0 \sin\phi_0$$

$$= \mu_L \dot{w} \left(\left(\frac{a \cos^3\phi_0}{b - (R_p + R_r + a)\sin\phi_0} \right) + \phi_0 \ln\left(1 + \frac{a}{R_r}\right) \sin^2\phi_0 \right) \tag{46}$$

The final point to consider involves the jump in shear stress across the **a**-lines on the upper and lower surfaces of the strip. S may vary through the thickness of the sheet or it may be constant. But, in order to satisfy the surface boundary conditions, S must drop to zero at the upper and lower surfaces. The shear stress expression must, therefore, contain a Heaviside step function of the form

$$S(\eta)\{H(\eta) - H(\eta - a)\}$$

and its first derivative will take the form $\frac{\partial S(\eta)}{\partial \eta}\{H(\eta)-H(\eta-a)\}+S(\eta)\{\delta(\eta)-\delta(\eta-a)\}$

where δ is the delta function.

In section CDGH, using equation (39)

$$\frac{\partial S_3}{\partial \eta}=\frac{-\mu_L \dot{w} \sin \phi_0}{(R_r+\eta)^2}\{H(\eta)-H(\eta-a)\}+\frac{\mu_L \dot{w} \sin \phi_0}{(R_r+\eta)}\{\delta(\eta)-\delta(\eta-a)\} \qquad (47)$$

Now $r=-(R_r+\eta)$ and substituting (47) into the first equation of (19) leads to

$$T_3=\frac{\mu_L \phi \dot{w} \sin \phi_0}{(R_r+\eta)}\{H(\eta)-H(\eta-a)\}+\mu_L \phi \dot{w} \sin \phi_0\{\delta(\eta)-\delta(\eta-a)\} \qquad (48)$$

The stress in the sheet along the fibre direction increases from zero at line DG up to a maximum value at $\phi=\phi_0$. It is infinite at both surfaces and is tensile within the sheet. The stress is tensile on the lower surface and on the upper surface it is compressive. A finite load is carried by the surface fibres, which have an infinitesimal thickness. Such a result is characteristic for solutions involving inextensible fibres. In reality, most of the stress is carried near the surface of the sheet during forming. This result is supported by Soll and Gutowski's work [19] on bending of thermoplastic composite beams. The second equation of (19) can then be used to solve for p.

$$p_3=\frac{\mu_L \phi \dot{w} \sin \phi_0}{(R_r+\eta)}\left[\ln\left(1+\frac{a}{R_r}\right)-\ln\left(1+\frac{\eta}{R_r}\right)\right]-\frac{\mu_L \phi \dot{w} \sin \phi_0}{(R_r+\eta)}\{H(\eta)-H(\eta-a)\} \qquad (49)$$

In the straight section BCHI, S is constant through the thickness of the sheet; so, equation (37) yields

$$\frac{\partial S_2}{\partial \eta}=\mu_L \dot{w}\left(\frac{\cos^2 \phi_0}{b-(R_p+R_r+a)\sin \phi_0}\right)\{\delta(\eta)-\delta(\eta-a)\} \qquad (50)$$

and using the first equation of (18) with k_a=0 leads to

$$T_2 = \mu_L \dot{w}(\ell_2 - \xi)\left(\frac{\cos^2\phi_0}{b - (R_p + R_r + a)\sin\phi_0}\right)\{\delta(\eta) - \delta(\eta - a)\} + T_{3_{max}} \tag{51}$$

where the arc length, ξ, is measured from line BI and

$$T_{3_{max}} = \frac{\mu_L \phi_0 \dot{w} \sin\phi_0}{(R_r + \eta)}\{H(\eta) - H(\eta - a)\} + \mu_L \phi_0 \dot{w} \sin\phi_0 \{\delta(\eta) - \delta(\eta - a)\} \tag{52}$$

The stress inside the sheet remains tensile for the duration of forming. The surface stresses reach their maximum values at line BI when ξ=0. The fibres are most likely to buckle on the upper surface at the point where the strip leaves the nose of the punch. The pressure term, p_2, in this region can be calculated using the second equation of (18) with k_a=0.

$$p_2 = \text{constant} = 0 \tag{53}$$

Under the punch nose the shear stress is zero and the first equation of (19) gives

$$T_1 = \text{const} = \mu_L \dot{w} \cos\phi_0 \{\delta(\eta) - \delta(\eta - a)\} + T_{3_{max}} \tag{54}$$

Finally p_1 may be calculated in the region ABIJ with r=(R_p+a-η) and S=0.

$$p_1 = \frac{\mu_L \phi_0 \dot{w} \sin\phi_0}{(R_p + a - \eta)} \ln\left(1 + \frac{\eta}{R_r}\right) + \mu_L \dot{w}\left(\cos\phi_0 + \phi_0 \sin\phi_0\right)\{H(\eta) - H(\eta - a)\} \tag{55}$$

The pressure terms (p_1 and p_3) normal to the **a**-lines are not constant through the thickness of the sheet and they cause spreading in the transverse fibre direction unless a stress, σ_{33}=-p, is applied to the strip. The plane strain condition is otherwise violated.

3 Experimental Procedure

In the course of this investigation, unidirectional preconsolidated PLYTRON sheets were cut into strips according to the dimensions shown in Figure 7. These were placed onto the holding jig, which was subsequently positioned in the bending apparatus illustrated in Figure 8. The experimental setup was placed into an environmental chamber so that the forming could be carried out at a constant elevated temperature. The strips were then free formed under three point bending into curved sections at speeds ranging from 50-500mm/min. The base of the forming apparatus was mounted on the Instron crosshead so that it could be moved upwards, thereby forcing the upper V-shaped die to form the PLYTRON strips downwards, and the final magnitude of deflection was kept constant.

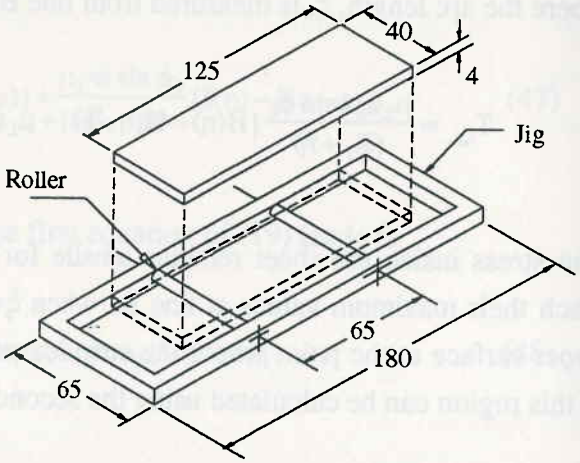

Figure 7: Holding jig and composite strip.

The upper die was attached to a 5kN load cell and the forming loads were measured in relation to the displacement of the crosshead. Small loads could be measured accurately by setting the load cell to read 20N/volt. To ensure thermal equilibrium during a test, at least 2hrs of heating was required to heat up the large mass of metal in the environmental chamber. The oven temperature was controlled by an independent Gefran 1000 PID controller, connected to a thermocouple placed inside the oven. Thus, the forming temperature could be set and maintained to within one degree celcius.

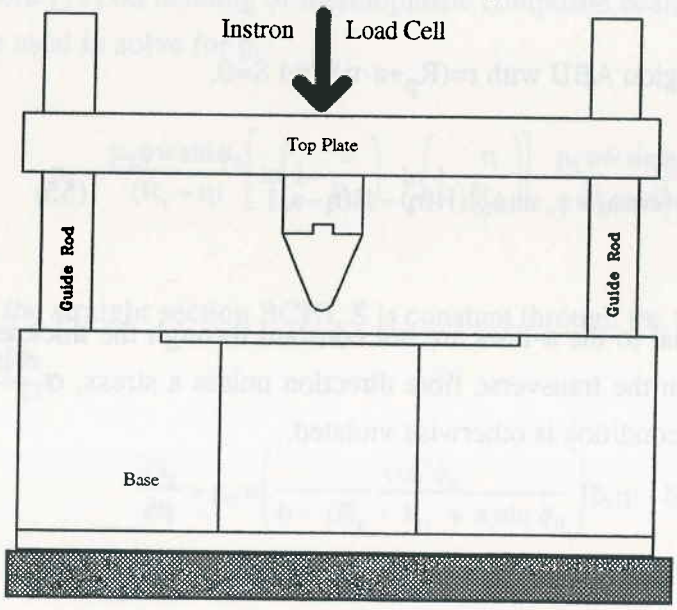

Figure 8: Schematic diagram of the V-bend apparatus.

The controller had a self-tuning option, which allowed it to evaluate the differential/integral control parameters such that the oven could be heated up without overshooting the preset temperature. Another thermocouple placed on the metal block base measured the die temperature, as this was critical to avoid large amounts of radiation to/from the specimen inside the oven. As soon as the whole apparatus had been pre-heated to the desired temperature, the specimen was placed onto the forming jig and positioned in the lower die block. The oven was then allowed to heat back to the pre-set temperature and the surface temperature of the specimen was monitored until an equilibrium temperature had been reached. Once the strip was ready to be formed, the cross-head was started and the specimen temperature, as well as the forming load, were recorded on a computer using an IBM ATOD board. In addition, the shape of the deformed part was observed in order to understand the way in which the specimen behaved during deformation.

4 Results and Discussion

One of the most notable features about free forming unidirectional PLYTRON sheets into V-bends was the consistent shape taken up by the strips as a result of the deformation. Figure 9 illustrates a typical section after complete forming and solidification.

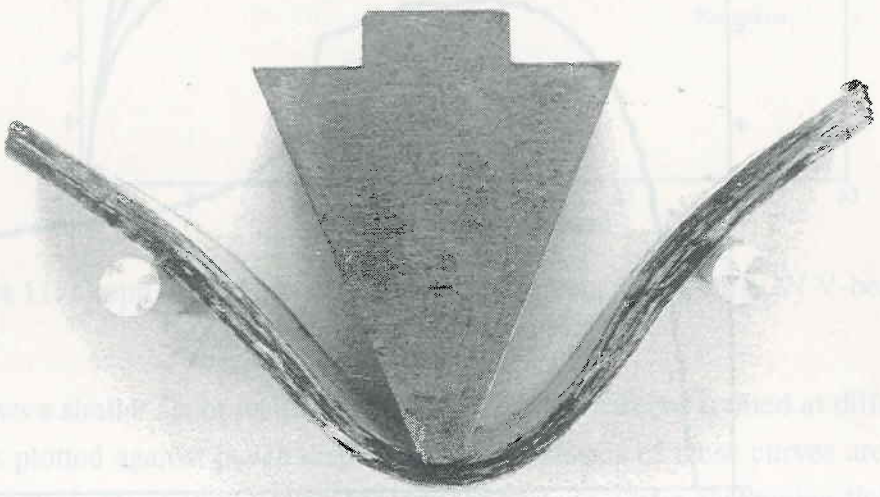

Figure 9: Cross-section of a free formed V-bend. Forming speed = 100mm/min.

In the initial stages of the deformation, both ends outside the supports remained flat and the central region began to deflect into a triangular shape. This happened for only a few millimetres of deflection before both ends of the strip began to lift up as it was drawn inwards. The middle portion then acquired a curvature much greater than that of the upper die. As the

sheet was pulled in between the supporting rollers, the ends continued to rotate and shear. This result was unexpected in light of the theoretical bending model, since there was no shear force acting on the sheet outside of the load supports. The degree of shear deformation outside of the supports is indicated by the angle of slip between the fibre layers at both ends One possible explanation for this is that the fibre layers retained some elastic flexural rigidity which caused them to deform by flexure rather than by shear. It is also worth noting that most of the shear deformation occurred in the resin rich regions between the layers.

In all of the specimens, the greatest amount of transverse spreading occurred at the punch nose. An increase in strip width of approximately 10% was typical in this region. The viscous beam bending model employed a plane strain constraint condition to simplify the analysis. This assumption is valid only if a stress equal to the pressure, -p, is applied at the edges of the sheet to prevent transverse spreading. In practice there was no side force on the specimens during forming, so the composite strips spread out in the transverse fibre direction.

Figure 10 shows the first set of experimental results for the load required to form a PLYTRON strip at an elevated temperature and a constant speed. In this case the load is plotted against time so that the relaxation effects in the material may be seen.

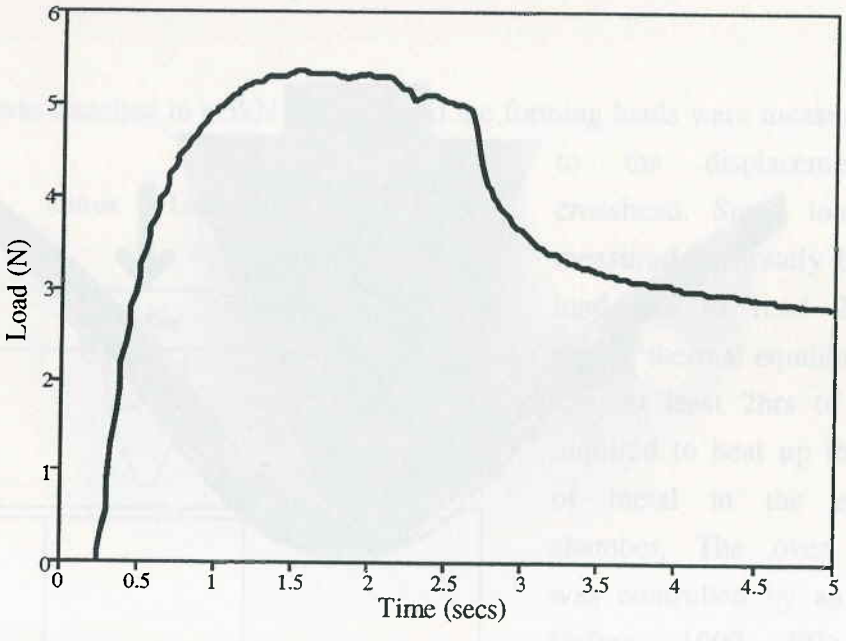

Figure 10: Graph of load against time for a PLYTRON V-bend.
Forming speed = 500mm/min, Temperature = 169.5°C.

The load rises from zero as the punch forces the strip downwards. This happens for a very small amount of the deflection before the load reaches a maximum value and thereafter slowly declines with increasing depth of penetration. The gradual decrease in load after reaching a peak value does not necessarily indicate a yield phenomenon in the material. It is more likely

that the shear rate decreases with increasing punch depth so that the viscous stresses diminish. In other words, it is a purely geometric effect. In this example, a load of only 5N was required to completely form the sheet. This demonstrates the ease with which thermoplastic composites may be moulded when they are soft. After about 2.5 seconds the crosshead was stopped. At this point the load dropped almost instantaneously and then continued to decrease asymptotically towards 2.5N. Such a result clearly indicates the degree of elasticity retained in PLYTRON at 169.5°C. If the material were truly viscous, the load would have dropped to zero as soon as the crosshead movement ceased. Instead, a considerable proportion of the load still remained on the punch after it was halted. The asymptotic relaxation load reached after a short period of time reflects the degree of elasticity retained by the polymer. The relaxation curve reveals a viscoelastic material response. For a few specimens, which were taken out of the forming apparatus before they had fully cooled, a noticeable amount of elastic recovery occurred. The long term relaxation modulus of PLYTRON is not quantifiable from these results, but it seems reasonable to describe the material as a viscoelastic fluid at temperatures near the top of the polymer's melting range.

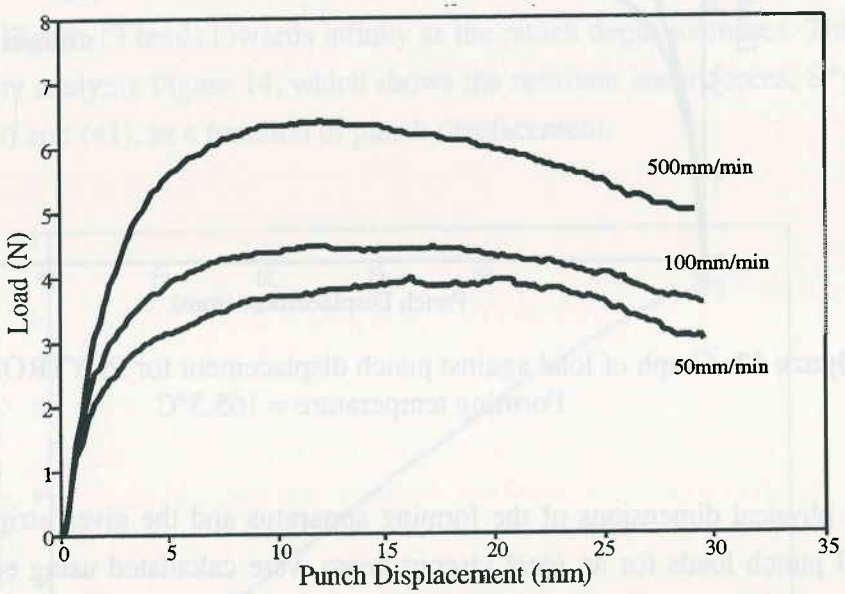

Figure 11: Graph of load against punch displacement for PLYTRON V-bends.
Forming temperature = 168.5°C

Figure 11 shows a similar set of results for three identical specimens formed at different speeds with the loads plotted against punch displacement. The shapes of these curves are self-similar and follow the same rise and fall trend previously mentioned. For a Newtonian fluid, the loads should be proportional to the forming speed. This is clearly not the case here. An increase in forming speed from 50mm/min to 500mm/min results in a load increase of about 20%. In addition, the load/displacement curve at 500mm/min differs slightly in shape from the other

two. These findings indicate a shear thinning phenomenon; therefore, a non-linear viscoelastic characterisation of the material is needed.

Figure 12 provides a comparison with Figure 11 for two specimens formed at different speeds and at a slightly lower temperature. Again the results are repeatable; however, the lower forming temperature causes an increase in the forming load. The fact that PLYTRON's rheological properties are strongly temperature dependent can be seen by comparing Figures 10, 11, and 12. Accurate temperature measurement is crucial when establishing PLYTRON material properties in this temperature range.

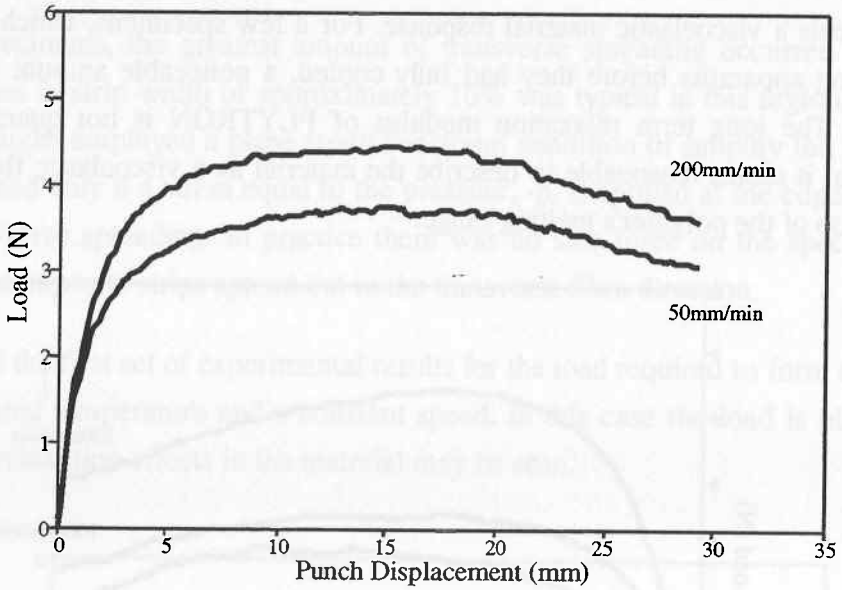

Figure 12: Graph of load against punch displacement for PLYTRON V-bends. Forming temperature = 165.5°C

Using the physical dimensions of the forming apparatus and the given strip dimensions, some theoretical punch loads for an ideal viscous beam were calculated using equation (46) Three load curves are illustrated in Figure 13 as a function of the punch displacement, w, for various forming speeds. Because the beam model assumes a Newtonian fluid constitutive relationship, the punch load varies linearly with punch speed. A comparison of these loads, at the beginning of the deformation, with the experimental loads suggests that the longitudinal viscosity of PLYTRON at 170°C lies in the range of 6000-10000 Pa.s.

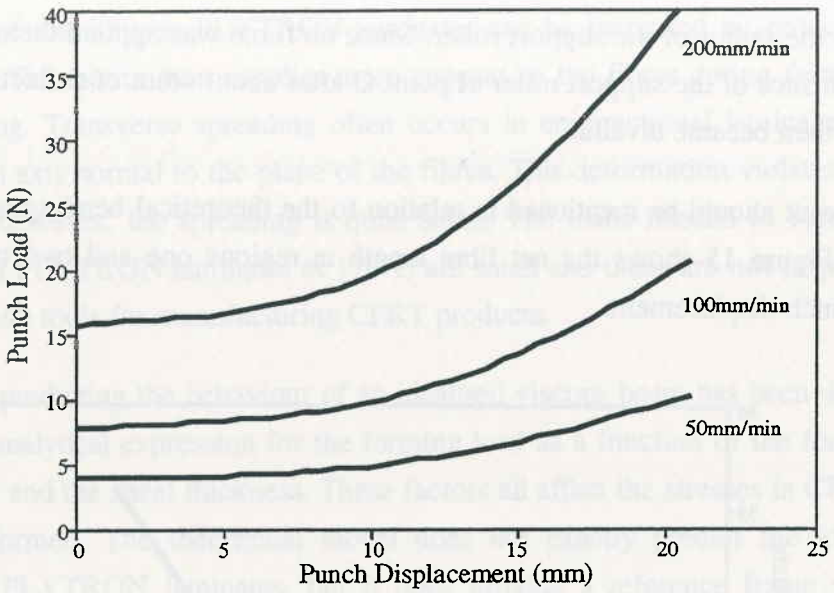

Figure 13: Punch load versus displacement for an ideal beam.
Strip width = 40mm, b = 32.5mm, a = 4mm, R_r = 2mm, R_p= 4mm, μ_L=8000Pa.s

The punch load in Figure 13 tends towards infinity as the punch depth increases. This outcome may be explained by studying Figure 14, which shows the resultant shear forces, S^*_2 and S^*_3, from equations (40) and (41), as a function of punch displacement.

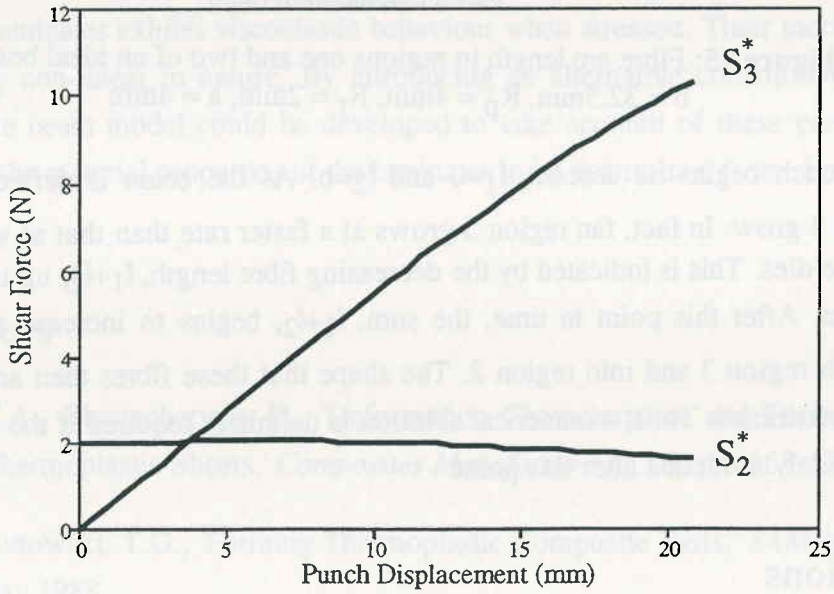

Figure 14: Resultant shear forces as a function of punch displacement.
Strip width = 40mm, b = 32.5mm, a = 4mm, R_r = 2mm, R_p= 4mm, μ_L=8000Pa.s

After a displacement of only a few millimetres S^*_3 becomes greater than S^*_2. This implies a negative jump in shear stress across line CH in Figure 5. Therefore, in order for the strip to continue to deform in a similar mode, a point load must be applied at point C to force the strip

to conform to the radius of the support roller. Since no force was applied there in practice, the strip left the surface of the support roller at point C after about 4mm of deflection and the load equation (46) then became invalid.

One further point should be mentioned in relation to the theoretical bending model developed in section 2. Figure 15 shows the net fibre length in regions one and two of the strip as a function of punch displacement.

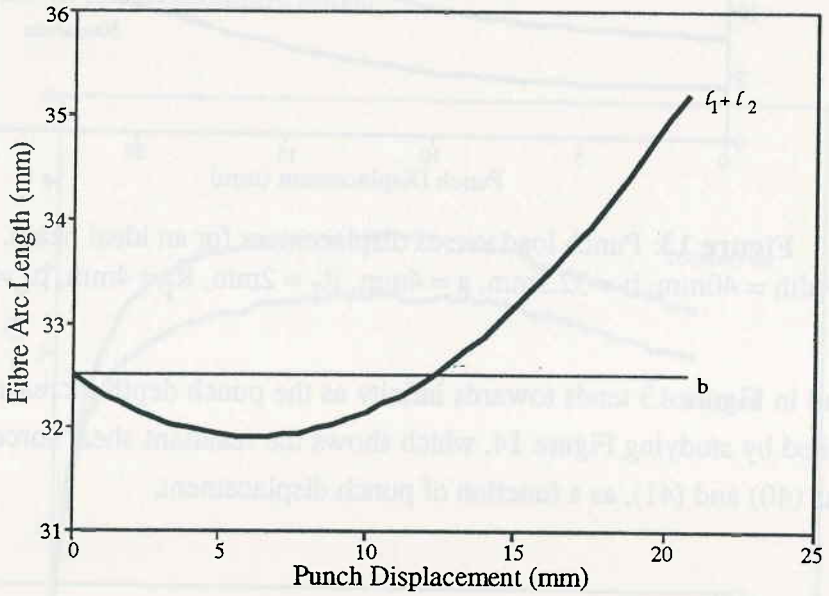

Figure 15: Fibre arc length in regions one and two of an ideal beam.
$b = 32.5mm$, $R_p = 4mm$, $R_r = 2mm$, $a = 4mm$

Before the punch begins its descent, $\ell_1=0$ and $\ell_2=b$. As the beam is deflected, the fans in regions 1 and 3 grow. In fact, fan region 3 grows at a faster rate than that at which the strip is drawn into the dies. This is indicated by the decreasing fibre length, $\ell_1+\ell_2$, up to a punch depth of about 5mm. After this point in time, the sum, $\ell_1+\ell_2$, begins to increase as the fibres are drawn through region 3 and into region 2. The shape that these fibres then acquire cannot be analytically determined. Thus, a numerical solution is definitely required if the forming process is to be adequately modelled after this point.

5 Conclusions

Forming V-bends allows the interlaminar shear properties of CFRT sheets to be isolated and studied. This forming mechanism is very important, when forming 3-D components, as the individual fibre layers must shear relative to one another.

The degree of elasticity in PLYTRON laminates can be increased by reducing the forming temperature. The matrix then supplies more support to the fibres during forming and inhibits fibre wrinkling. Transverse spreading often occurs in unidirectional laminates when they are bent along an axis normal to the plane of the fibres. This deformation violates the plane strain assumption; however, the spreading is quite small. The loads needed to form V-bends from unidirectional PLYTRON laminates at 170°C are small and these are not of prime importance when designing tools for manufacturing CFRT products.

A model for predicting the behaviour of an idealised viscous beam has been developed, which provides an analytical expression for the forming load as a function of the forming speed, the die geometry and the sheet thickness. These factors all affect the stresses in CFRT materials as they are deformed. The theoretical model does not exactly predict the load/displacement response of PLYTRON laminates, but it does provide a reference frame within which to interpret the experimental bending results. It also establishes a useful basis for further theoretical work on kinematically constrained models, which render relatively simple solutions to complex forming problems. The simple shear deformations between layers of fibres in CFRT laminates are characterised particularly well by the bending model. Unfortunately an analytical solution for large deflections has not been obtained. However, there is no reason why a numerical solution cannot be generated by using the same fundamental assumptions about the deformation.

PLYTRON laminates exhibit viscoelastic behaviour when stressed. Their mechanical response is also highly non-linear in nature. By introducing an alternative constitutive relationship, a more accurate beam model could be developed to take account of these peculiarities, which would allow the material properties of the laminates to be determined from simple bend tests in the future.

6 References

1. Martin, T.A., Bhattacharyya, D., 'Deformation Characteristics and Formability of Fibre-Reinforced Thermoplastic Sheets,' *Composites Manufacturing*, 3/3, pp. 165-172, 1992.

2 Soll, W., Gutowski, T.G., 'Forming Thermoplastic Composite Parts,' *SAMPE Journal*, 24/3, pp. 15-19, May 1988.

3 Tam, A.S., Gutowski, T.G., 'Ply-Slip During the Forming of Thermoplastic Composite Parts,' *Journal of Composite Materials*, 23, pp. 587-605, June 1989.

4 Friedrich, K., Hou, M., 'Stamp Forming of Continuous Carbon Fibre/Polypropylene Composites,' *Composites Manufacturing*, 2/1, pp. 3-9, Mar 1991.

5 Rogers, T.G., Bradford, I.D.R., England, A.H., 'Finite Plane Deformations of Anisotropic Elastic-Plastic Plates and Shells,' *Journal of Mech. Phys. Solids*, 40/7, pp. 1595-1606, 1992.

6 Bradford, I.D.R., England, A.H., Rogers, T.G., 'Finite Deformations of a Fibre-Reinforced Cantilever: Point-Force Solutions,' *Acta Mechanica 91*, pp. 77-95, 1992.

7 Evans, J.T., 'A Simple Continuum Model of Creep in a Fibre Composite Beam,' *Journal of Applied Mechanics, Transactions of the ASME*, 60, pp. 190-195, 1993.

8 Rogers, T.G., O'Neill, J.M., 'Theoretical Analysis of Forming Flows of Fibre-Reinforced Composites,' *Composites Manufacturing*, Vol. 2, 3/4, pp. 153-160, 1991.

9 Spencer, A.J.M., 'Deformations of Fibre-Reinforced Materials,' *Oxford University Press*, London, 1972.

10. Pipkin, A.C., Rogers, T.G., 'Plane Deformations of Incompressible Fibre Reinforced Materials,' *Journal of Applied Mechanics (Transactions of the ASME)*, pp. 634-640, Sept 1971.

11. Rogers, T.G., 'Rheological Characterization of Anisotropic Materials,' *Composites*, 20/1, pp. 21-27, Jan 1989.

12 Johnson, W., Sowerby, R. and Haddow, J.B., 'Plane-Strain Slip-Line Fields' Edward Arnold Ltd., pp. 27, 1970.